Proceedings of the ASME 2012 International Design Engineering Technical Conferences &
Computers and Information in Engineering Conference
IDETC/CIE 2012
August 12-15, 2012, Chicago, IL, USA

DETC2012-71064

FIRST INDUSTRIAL STRENGTH MULTI-AXIAL ROBOTIC TESTING CAMPAIGN FOR COMPOSITE MATERIAL CHARACTERIZATION

John G. Michopoulos
Computational Multiphysics Systems Lab.
Center of Computational Material Science
Naval Research Laboratory
Washington DC 20375, USA

John C. Hermanson
Wood Based Materials & Structures
Forest Products Laboratory
USDA Forest Service
Madison, WI, USA

Athanasios Iliopoulos
Computational Materials Science Center
George Mason University, Fairfax VA 22030, USA
resident at Center of Computational Material Science
Naval Research Laboratory
Washington DC 20375, USA

ABSTRACT

In this paper we are reporting on the first successful campaign of systematic, automated and massive multiaxial tests for composite material constitutive characterization. The 6 degrees of freedom system developed at the Naval Research Laboratory (NRL) called NRL66.3, was used for this task. This was the inaugural run that served as the validation of the proposed overall constitutive characterization methodology. It involved accomplishing performing I152 tests in 12 business days reaching a peak throughput of 212 tests per day. We describe the context of the effort in terms of the reasoning and the actual methods behind it. Finally, we present representative experimental data and associated constitutive characterization results for representative loading paths.

INTRODUCTION

During the past decade we have embarked in an effort to automate massive multiaxial testing of composite coupons in order to determine the constitutive behavior of the bulk composite material used to make these coupons. In this paper we are reporting on the first successful campaign of experiments for this purpose. The approach is motivated by the data-driven requirements of employing design optimization principles for determining the constitutive behavior of composite materials as described in our recent work [1,2] The constitutive characterization of composite materials has been traditionally achieved through conventional uniaxial tests and used for determining elastic properties. Typically, extraction of these properties, involve uniaxial tests conducted with specimens mounted on uniaxial testing machines, where the major orthotropic axis of any given specimen is angled relative to the loading direction. In addition, specimens are designed such that a homogeneous state of strain is developed over a well defined area, which is for the purpose of measuring kinematic quantities [3,4]. Consequently, the use of uniaxial testing machines imposes requirements of using multiple specimens, griping fixtures and multiple experiments. The requirement of a homogeneous state of strain frequently imposes restrictions on the sizes and shapes of specimens to be tested.

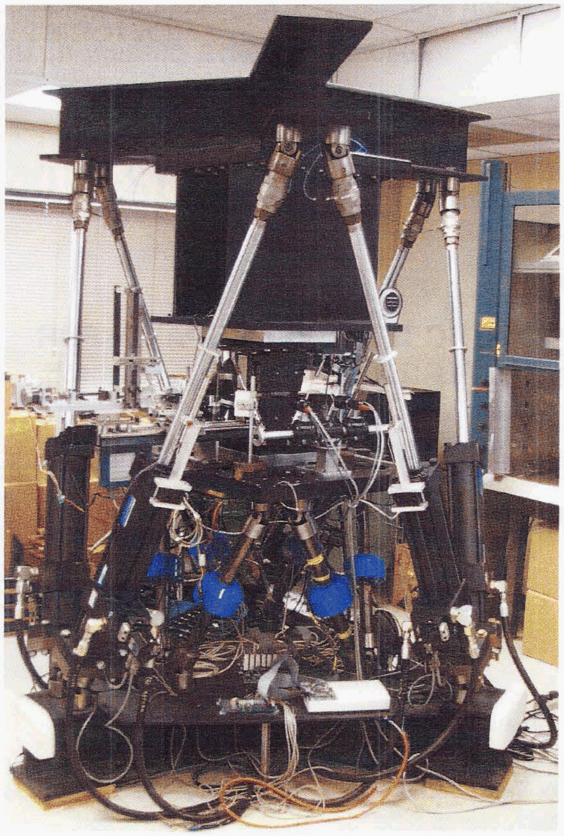

FIGURE 1: VIEW OF CURRENT STATE OF THE NRL66.3. A 6-DOF MECHATRONICALLY AUTOMATED SYSTEM FOR THE MULTI-AXIAL TESTING OF COMPOSITE MATERIALS

Consequently, these requirements result in increased cost and time, and consequently to inefficient characterization processes. To address these issues and to extend characterization to non-linear regimes, multi-degree of freedom automated mechatronic testing machines, which are capable of loading specimens multiaxially in conjunction with energy-based inverse characterization methodologies, were introduced at the Naval Research Laboratory (NRL) [5–7]. This introduction was the first of its kind and has continued through the present [8–10]. The most recent prototype of these machines, which is currently under verification, is shown in Fig. 1. The energy-based approach associated with mechatronic testing, although it enables multiaxial loading and inhomogeneous states of strain, still requires multiple specimens. It is significant to state however, that these specimens are tested in an automated manner with high throughput of specimens per hour, which have reached values of 28 specimens per hour. The recent development of flexible full-field displacement and strain measurements methods has afforded the opportunity of alternative characterization methodologies [11-14]. Full-field optical techniques, such as Moire and Speckle Interferometry, Digital Image Correlation (DIC), and Meshless Random Grid Method (MRGM), which measure displacement and strain fields during mechanical tests, have been used mostly for elastic characterization of various materials [14-17]. The resulting measurements are used for identification of constitutive model constants, via the solution of an appropriately formed inverse problem, with the help of various computational techniques. Arguably, the most popular methodology is the mixed numerical/experimental method that identifies the material's elastic constants by minimizing an objective function formed by the difference between the full-experimental measurements and the corresponding analytical model predictions via an optimization method [5–10, 14, 17–19]. Our focus in the present work is to describe recent efforts concerning design optimization methodologies for constitutive material characterization and in particular the first campaign of massive tests. Our approaches are based mostly on energy conservation arguments, and they can be classified according to computational cost in relation to the iterative use of FEA or not. It is important to clarify that digitally acquired images are processed by software [20] that implements the MRGM [14,21-25] and is used to extract the full-field displacement and strain field measurements as well as the boundary displacements required for material characterization. Reaction forces and redundant boundary displacement data are acquired from displacement and force sensors integrated with NRL's multiaxial loader called NRL66.3 [26]. In an effort to address the computational cost of the FEA-in-the-loop approaches, the authors have initiated a dissipated and total strain energy density determination approach that has recently been extended to a framework that is derived from the total potential energy and the energy conservation, which can be applied directly with full field strain measurement for characterization [27–32]. In the section that follows we present an overview of the small strain formulation (SSF) of the general strain energy density approach followed by the finite strain formulation (FSF), that are intended to capture both the linear and non-linear constitutive behavior of composite materials with or without damage. The paper continuous with a description of the computational application of design optimization implementations based on these two formulations. A description of he experimental campaign and representative results follow. Finally, conclusions are presented.

COMPOSITE MATERIAL CONSTITUTIVE RESPONSE REPRESENTATIONS

For the general case of a composite material system we consider that a modified anisotropic hyperelastic strain energy density function can be constructed to encapsulate both the elastic and the inelastic responses of the material. However, certain classes of composite materials reach failure after small strains and some under large strains. For this reason we give two examples, one involving a small (infinitesimal) strain formulation (SSF) and another involving an finite (large) strain formulation (FSF).

Small Strain Formulation For the SSF we introduce a SED function that, in its most general form, can be represented as a scaled Taylor expansion of the Helmholtz free energy of a deformable body, which is in terms of small strain invanants of the form.

$$
\begin{aligned}
U_{SSF}(I_1,I_2,I_3) = s_0 + s_{11}I_1 + \frac{1}{2}s_{12}I_1^2 + \frac{1}{3!}s_{13}I_1^3 + \\
+\frac{1}{4!}s_{14}I_1^4 + \ldots + s_{21}I_2 + \frac{1}{2}s_{22}I_2^2 + \frac{1}{3!}s_{23}I_2^3 + \\
+\frac{1}{4!}s_{24}I_2^4 + \ldots + \frac{1}{2}s_{13}I_3^2 + \frac{1}{3!}s_{13}I_3^3 + \frac{1}{4!}s_{14}I_3^4 + \\
\ldots + \frac{1}{2}s_{1121}I_1I_2 + \frac{1}{3!}s_{1221}I_1^2I_2 + \frac{1}{3!}s_{1122}I_1I_2^2 + \ldots \\
+\frac{1}{2}s_{1131}I_1I_3 + \frac{1}{3!}s_{1331}I_1^2I_3 + \frac{1}{3!}s_{1133}I_1I_3^2 + \ldots + \\
\frac{1}{4!}s_{1321}I_1^3I_2 + \frac{1}{4!}s_{1221}I_1^2I_2^2 + \frac{1}{4!}s_{1123}I_1I_2^3 + \ldots,
\end{aligned}
\tag{1}
$$

where the invariants are defined by:

$$
\begin{aligned}
I_1 &= tr(\varepsilon) = \varepsilon_{ii}, \\
I_2 &= \frac{1}{2}tr(\varepsilon^2) = \frac{1}{2}\varepsilon_{ij}\varepsilon_{ij}, \\
I_3 &= \frac{1}{2}tr(\varepsilon^3) = \frac{1}{3}\varepsilon_{ij}\varepsilon_{jk}.\varepsilon_{ki}.
\end{aligned}
\tag{2}
$$

The invariants are chosen to take advantage of a priori knowledgethat the SED as a scalar quantity,must be invariant under frame reference translations and rotations. This follows in that the SED should be objective (i.e. independent of the observer's frame of reference). An additive decomposition of this expression in terms of a recoverable and an irrecoverable SED can be expressed by:

$$
U_{SSF} = U^R_{SSF}(S;\varepsilon_{ij}) + U^I_{SSF}(D;\varepsilon_{ij}). \tag{3}
$$

Clearly, all the second order monomials of strain components will be forming the recoverable part $U^R_{SSF}(S;\varepsilon_{ij})$ and the higher order monomials will be responsible for the irrecoverable part $U^I_{SSF}(D;\varepsilon_{ij})$. The resulting constitutive law is given by:

$$
\begin{aligned}
\sigma_{ij} = \partial U_{SSF}/\partial\varepsilon_{ij} = \partial(U^R_{SSF}(S;\varepsilon_{ij}) + U^I_{SSF}(D;\varepsilon_{ij}))/\partial\varepsilon_{ij} = \\
= \frac{\partial U_{SSF}}{\partial I_1}\frac{\partial I_1}{\partial\varepsilon_{ij}} + \frac{\partial U_{SSF}}{\partial I_2}\frac{\partial I_2}{\partial\varepsilon_{ij}} + \frac{\partial U_{SSF}}{\partial I_3}\frac{\partial I_3}{\partial\varepsilon_{ij}}.
\end{aligned}
\tag{4}
$$

A general expression which provides a strain dependent version of Eq. 3, is given by,

$$
\begin{aligned}
U_{SSF} = U^R_{SSF}(S;\varepsilon_{ij}) + U^I_{SSF}(D;\varepsilon_{ij}) = \\
= \frac{1}{2}s_{ijkl}\varepsilon_{ij}\varepsilon_{kl} + d_{ijkl}(\varepsilon_{ij})\varepsilon_{ij}\varepsilon_{kl},
\end{aligned}
\tag{5}
$$

where s_{ijkl} are the components of the elastic stiffness tensor (Hooke's tensor) and $d_{ijkl}(\varepsilon_{ij})$ are strain-dependent damage functions, which fully define irrecoverable or dissipated strain energy density given by enforcing the dissipative nature of energy density. The quantity d_{ijkl} (ε_{ij}) can be defined in a manner analogous to that employed for the 1D system described above and is given by:

$$
d_{ijkl}(\varepsilon_{ij}) = s_{ijkl}(1 - e^{(-\frac{\varepsilon_{ij}}{q_{ij}})^{p_{ij}}/(ep_{ij})}). \tag{6}
$$

We perform an equivalent series expansion and subsequently drop all terms except the first, in that it captures almost all of the dissipative behavior. Accordingly:

$$
\begin{aligned}
d_{ijkl}(\varepsilon_{ij}) = s_{ijkl}\sum_{m=1}^{n}(-1)^m\left(\frac{1}{ep_{ij}}\right)^m \frac{\varepsilon_{ij}^{mp_{ij}}}{m!q_{ij}^{mp_{ij}}} = \\
= s_{ijkl}(-\left(\frac{1}{ep_{ij}}\right)\frac{\varepsilon_{ij}^{p_{ij}}}{q_{ij}^{p_{ij}}} + \left(\frac{1}{ep_{ij}}\right)^2\frac{\varepsilon_{ij}^{2p_{ij}}}{2q_{ij}^{2p_{ij}}} - \cdots +) \simeq \\
\simeq -s_{ijkl}\left(\frac{1}{ep_{ij}}\right)\frac{\varepsilon_{ij}^{p_{ij}}}{q_{ij}^{p_{ij}}}.
\end{aligned}
\tag{7}
$$

Thus the irrecoverable part of the energy in Eq. 3 becomes:

$$
\begin{aligned}
U^I_{SSF}(D;\varepsilon_{ij}) = U^I_{SSF}(s_{ijkl},p_{ij},q_{ij};\varepsilon_{ij}) = \\
= -s_{ijkl}\frac{1}{e(2+p_{ij})p_{ij}q_{ij}^{p_{ij}}}\varepsilon_{ij}^{1+p_{ij}}\varepsilon_{kl}.
\end{aligned}
\tag{8}
$$

Next, substituting Eq. 6 into Eq. 3 yields:

$$
\begin{aligned}
U_{SSF} = U^R_{SSF}(S;\varepsilon_{ij}) + U^I_{SSF}(D;\varepsilon_{ij}) = \\
= \frac{1}{2}s_{ijkl}\varepsilon_{ij}\varepsilon_{kl} - s_{ijkl}\frac{1}{e(2+p_{ij})p_{ij}q_{ij}^{p_{ij}}}\varepsilon_{ij}^{1+p_{ij}}\varepsilon_{kl}.
\end{aligned}
\tag{9}
$$

Applying Eq. 2 on Eq. 7, and employing Voight [3] notation for the case of a general orthotropic material, yields the constitutive relation,

$$\begin{bmatrix}\sigma_{xx}\\ \sigma_{yy}\\ \sigma_{zz}\\ \sigma_{xz}\\ \sigma_{yz}\\ \sigma_{xy}\end{bmatrix} = \begin{bmatrix} \breve{s_{xx}} & s_{xy} & s_{xz} & 0 & 0 & 0\\ s_{xy} & \breve{s_{yy}} & s_{yz} & 0 & 0 & 0\\ s_{xz} & s_{yz} & \breve{s_{zz}} & 0 & 0 & 0\\ 0 & 0 & 0 & \breve{s_{xz}} & 0 & 0\\ 0 & 0 & 0 & 0 & \breve{s_{yz}} & 0\\ 0 & 0 & 0 & 0 & 0 & \breve{s_{xy}}\end{bmatrix}\begin{bmatrix}\varepsilon_{xx}\\ \varepsilon_{yy}\\ \varepsilon_{zz}\\ \varepsilon_{xz}\\ \varepsilon_{yz}\\ \varepsilon_{xy}\end{bmatrix}, \tag{10}$$

where,

$$\breve{s_{ij}} = s_{ij}\left(1-\bar{d_{ij}}\right) \tag{11}$$

and

$$\bar{d_{ij}} = \frac{1}{e p_{ij} q_{ij}^{p_{ij}}}\varepsilon_{ij}^{1+p_{ij}}. \tag{12}$$

All terms that are not shown in expression of Eq. 10 are zero due to the orthotropic symmetry requirements. Therefore, the material parameters are the 9 elastic s_{ij} constants and $6 \times 2 = 12$ damage constants p_{ij}, q_{ij} for a total of 21 parameters. Clearly, when the quantities $\bar{d_{ij}}$ do not depend on the strains and they are constants, Eq. 8 reduces to most of the continuous damage theories given by various investigators in the past [33–36]. For a transversely isotropic material the number of material parameters drops to 5+10=15 for a 3D state of strain and to 4+8=12 for a plane stress state.

Finite Strain Formulation The FSF can be written in a double additive decomposition manner. The first being the decomposition of the recoverable and irrecoverable SED, and the second being the decomposition between the volumetric (or dilatational) W_v and the distortional (or isochoric) W_d parts of the total SED. This decomposition is expressed by,

$$\begin{aligned} U_{SSF} &= U^R_{SSF}(\alpha_i; J, \bar{C}) + U^I_{SSF}(\alpha_i, \beta_i; J, \bar{C}) = \\ &= [W_v(J) + W_d(\bar{C}, A\otimes A, B\otimes B)] - \\ &- [d_v W_v(J) + d_d W_d(\bar{C}, A\otimes A, B\otimes B)], \end{aligned} \tag{13}$$

where α_i, β_i are the elastic and inelastic material parameters of the system, respectively. A rearrangement of these decompositions, such as the volumetric vs. distortional decomposition, which appears on the highest expression level, leads to an expression introduced in [37], i.e.,

$$U_{FSF} = (1-d_v)W_v(J) + (1-d_d)W_d(\bar{C}, A\otimes A, B\otimes B), \tag{14}$$

with the damage parameters $d_k \in [0,1], k \in [v,d]$ defined as,

$$d_k = d^{\infty}_{ka}\left[1 - e^{\left(-\frac{a_k(t)}{\eta_{ka}}\right)}\right], \tag{15}$$

where $a_k(t) = \max_{s\in[0,t]} W^o_k(s)$ is the maximum energy component reached so far, and $d^{\infty}_{ka}, \eta_{ka}$ are two pairs of parameters controlling the energy dissipation characteristic of the two components of SED. In this formulation, $J = \det \underline{F}$ is the Deformation Gradient, $\bar{C} = \underline{F}^T \underline{F}$ is the right Cauchy Green (Green deformation) tensor, A, B are constitutive material directions in the undeformed configuration, and $A\otimes A, B\otimes B$ are microstructure structural tensors expressing fiber directions. Each of the two components of SED are defined as,

$$\begin{aligned} W_v(J) &= \frac{1}{d}(J-1)^2 W_d(\bar{C}, A\otimes A, B\otimes B) = \\ &= \sum_{i=1}^{3} a_i(\bar{I}_1 - 3)^i + \sum_{j=1}^{3} b_j(\bar{I}_2 - 3)^j + \sum_{k=1}^{6} c_k(\bar{I}_4 - 1)^k + \\ &+ \sum_{l=2}^{6} d_l(\bar{I}_5 - 1)^l + \sum_{m=2}^{6} e_m(\bar{I}_6 - 1)^m + \sum_{n=2}^{6} f_n(\bar{I}_7 - 1)^n + \\ &+ \sum_{o=2}^{6} g_o(\bar{I}_8 - (A\cdot B)^2)^o, \end{aligned} \tag{16}$$

where the strain invariants are defined as follows:

$$\begin{aligned} &\bar{I}_1 = tr\bar{C},\ \bar{I}_2 = \tfrac{1}{2}(tr^2\bar{C} - tr\bar{C}^2) \\ &\bar{I}_4 = A\cdot\bar{C}B,\ \bar{I}_5 = A\cdot\bar{C}^2 B \\ &\bar{I}_6 = B\cdot\bar{C}B,\ \bar{I}_7 = B\cdot\bar{C}^2 B,\ \bar{I}_8 = (A\cdot B)A\cdot\bar{C}B. \end{aligned} \tag{17}$$

The corresponding constitutive behavior is given by the second Piola-Kirchhoff stress tensor according to [34]:

$$S = 2\frac{\partial U_{FSF}}{\partial C} \tag{18}$$

or the usual Cauchy stress tensor according to:

$$\sigma_{FSF} = \frac{2}{J}F\cdot\frac{\partial U_{FSF}}{\partial C}\cdot F^T. \tag{19}$$

Under the FSF formulation the material characterization problem involves determining the *36* coefficients (at most) of all monomials when the sums in the expression of distortional SED are expanded in Eq. **16,** in addition to the compressibility constant d and the 4 parameters used in Eq. *15.* It follows that potentially there can be a total of 41 material constants.

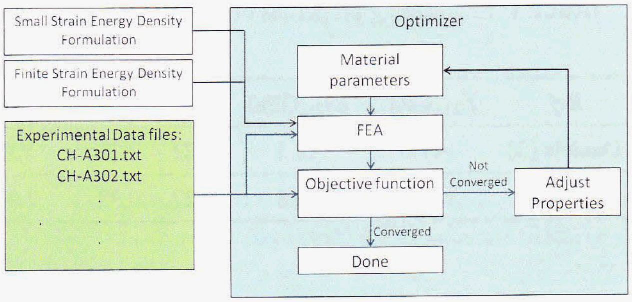

FIGURE 2: OVERVIEW OF DESIGN OPTIMIZATION LOGIC IMPLEMENTATION

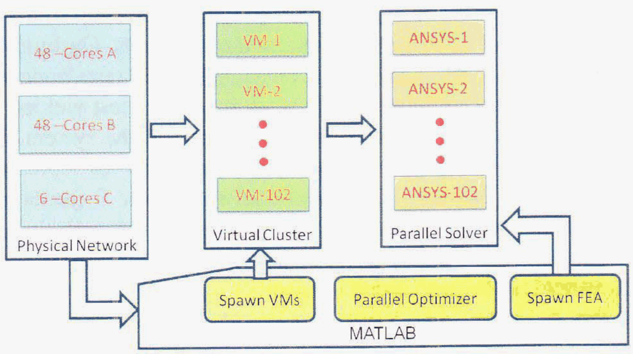

FIGURE 3: VIRTUALIZED COMPUTE CLUSTER ARCHITECTURE FOR IMPLEMENTING THE OPTIMIZATION IN PARALLEL

COMPUTATIONAL IMPLEMENTATION

In order to determine the material parameters the inverse problem at hand is solved through a design optimization approach that is described by the logic depicted in Fig. 2. The implementation of this logic involved a computational infrastructure that controlled by Matlab, where the foreword solution of the instantaneous FEA was accomplished by ANSYS. Due to the costly calculations we created a virtual cluster that essentially used the multiple cores available in three systems, via a spawning 102 virtual machines capable of running 102 instances of ANSYS in a parallel fashion, whereas each process was responsible for a different subdomain of the design space. An overview of the adopted architecture is shown in Fig, 3. Details if the FEM model used for the specimens constructed and tested are not presented here due to the space limitations but they can be found in [1,2]. Two objective functions were constructed. Both utilized the fact that through the REMDIS-3D software [38], developed by our group, one can obtain full field measurements of the displacement and strain fields over any deformable body as an extension of the REMDIS-2D software that is based on the MRGM [14,20-25]. Thus, our experimental measurements for

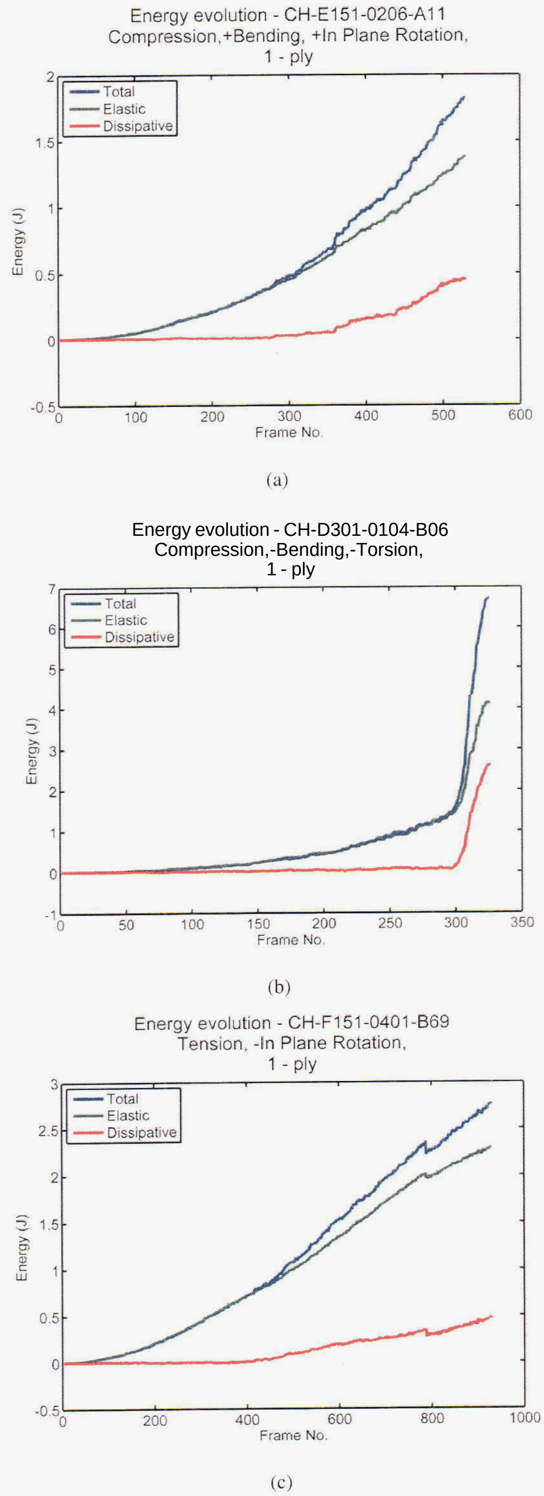

FIGURE 4: EVOLUTION OF TOTAL, ELASTIC AND DISSIPATED ENERGY FOR THREE DISTINCT LOAD PATHS

the formation of the objective functions were chosen to be the strains at the nodal points of the FEM discretization. The first objective function chosen was based entirely on strains and is given by,

$$J^{\varepsilon} = \sum_{k=1}^{N} \left(\sum_{i=1}^{2} \sum_{j=i}^{2} \left(\left[\varepsilon_{ij}^{\exp} \right]_k - \left[\varepsilon_{ij}^{fem} \right]_k \right) \right)^2, \quad (20)$$

the second objective function is given in terms of surface strain energy density according to,

$$J^{U} \approx \oint_{\partial\Omega} \left(U^{\exp} - U^{fem} \right)^2 dS \approx$$

$$\approx \oint_{\partial\Omega} \left(\sum_{i=1}^{2} \sum_{j=i}^{2} \sum_{m=1}^{2} \sum_{n=m}^{2} \left(s_{ijmn} \varepsilon_{ij}^{\exp} \varepsilon_{mn}^{\exp} - s_{ijmn} \varepsilon_{ij}^{fem} \varepsilon_{mn}^{fem} \right) \right)^2 dS. \quad (21)$$

where $\left[\varepsilon_{ij}^{\exp}\right]_k, \left[\varepsilon_{ij}^{fem}\right]_k$ are the experimentally determined and the FEM produced components of strain are at node k. The quantities U^{exp}, U^{fem} are the surface strain energy densities formulated by using the experimental strains and the FEM produced strains respectively. Both objective functions were implemented, and we utilized both the DIRECT global optimizer [39], which is available within Matlab [40], and a custom developed Monte-Carlo optimizer, also implemented in Matlab.

EXPERIMENTAL CAMPAIGN

Based on an analysis that falls outside the scope of the present paper [41], we identified 72 proportional loading paths to sample the 6-DoF space defined by the 3 translations and 3 rotations that can be applied by the moveable grip of the NRL66.3. We selected to use a single specimen per loading path and then repeat the process. That requires 144 specimens per material system. Each material system was a defined to be a balanced laminate with an alternating angle of fiber inclination per ply relative to the vertical axis of the specimen that is perpendicular to the axis defined by the two notches of the specimen. Four angles were used $+/-15, +/-30, +/-60, +/-75$ degrees and therefore $4 \times 144 = 576$ specimens were constructed. The actual material used to make the specimens was an AS4/3506-1 epoxy resin/fiber respectively.

However, because we needed to study ply thickness length scale effects, we constructed an equal amount of specimens where the cross-plied unidirectional laminas were made with 4 plies each, thus leading to thicker uniaxial laminas. This doubled the number of total specimens to 1152 and this was the final number of required tests. All specimens were tested

TABLE 1: Engineering properties of AS4/3506-1 laminae

Ref	E_{11}[GPa]	E_{22} [GPa]	ν_{12}	ν_{23}	G_{12}[GPa]
Daniels [3]	147.0	10.3	0.27	0.28	7.0
Present	125.0	10.8	0.27	0.32	7.96

by using NRL66.3 in May of 2011. A very small sample of the testing process is shown in a movie that can be found in the URL “http://www.youtube.com/watch?v=Cp18y3HAqsM”. In May 13, 2011, the system achieved a throughput of 20 test/hour for a total of 132 tests. On May 27 the system achieved a throughput of 25 tests/hour for a total of 216 tests. On June 15, 2011 the system reached its peak throughput of 28 tests/hour. All 1152 tests were completed in 12 work-days. The test yielded 13 TB of data from the sensors and the cameras of the system. Instead of presenting typical load-displacement curves representing collected data in a 12-dimensional space (i.e. 3 forces and 3 moments vs. 3 translations and 3 rotations respectively) we rather present total energy distribution as a function of load-increment (frame no.) along the respective loading path as shown in Fig. 4. Using the collected data and the optimization approach outlined earlier for the case of the SSF we identified the elastic constants as shown in Table 2, in comparison to those of [3]. By running FEA for the cases that correspond to the specific loading path corresponding to an experiment we can now compare the predicted distribution of any component of the strain or stress tensor. In order to demonstrate how well the FSF formulation can capture the behavior of the characterization coupons used to obtain the data utilized in the characterization process we are presenting typical examples in terms of the distributions of ε_{yy} as measured by the MRGM (left column) and as predicted by the FSF theory (right column), for both the front (top row) and the back (bottom row) of Figs. 5, 6, 7, and 8. It is important to indicate here that the characterization methodology described here and in our previous publications, utilized the data described herein along with the data form other validation tests performed on structures of different shape and layups than that of the characterization coupons, to perform validation comparisons. A discussion of this activity is presented in a companion paper submitted for publication in the present conference [42].

CONCLUSIONS AND PLANS

We have described the first industrial strength campaign of multiaxial experiments performed with the NRL66.3 mechatronic system.

The application of design optimization methodologies for the determination of the constitutive response of composite ma-

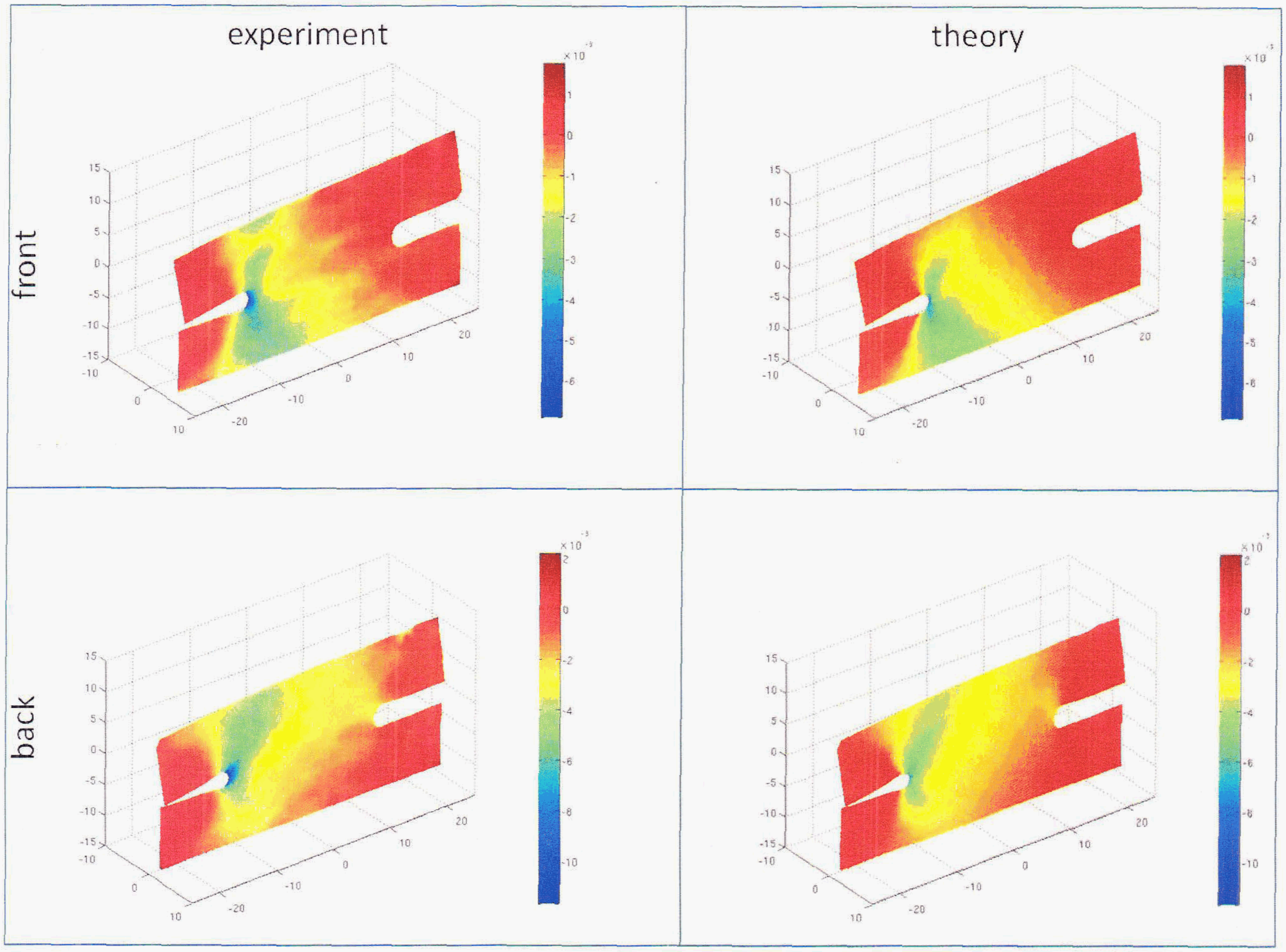

FIGURE 5: COMPARISON OF (ε_{yy}) FIELD BETWEEN MEASURED (LEFT) AND THE IDENTIFIED MODEL BY USING THE FSF FOR THE CASE OF COMPRESSION AND IN-PLANE ROTATION OF A +/- 30 DEGREES LAMINATE

terials with or without damage has been employed. Strain energy density and full field strain based approaches have been utilized to incorporate massive full field strain measurements from specimens loaded by a custom-made multiaxial loading machine. We have formulated objective functions expressing the difference between the experimentally observed behavior of composite materials under various loading conditions, and the simulated behavior via FEA, which are formulated in terms of strain energy density functions of a particular structure under identical loading conditions. Two formalisms involving small strains and finite strains have been utilized in a manner that involves both additive decomposition of recoverable and irrecoverable strain energy density. This was done in order to address both the elastic and inelastic response of composite materials due to damage. The finite strain formulation further involves a volumetric and distortional energy decomposition.

Representative results of the characterization have been compared with the associated experimental ones to demonstrate how well they agree.

ACKNOWLEDGMENT

The authors acknowledge support for this work by the Office of Naval Research and the Naval Research Laboratory's core funding.

REFERENCES

[1] Michopoulos, J., Hermanson, J., Iliopoulos, A., Lambrakos, S., and Furukawa, T., 2011. "Data-driven design optimization for composite material characterization".

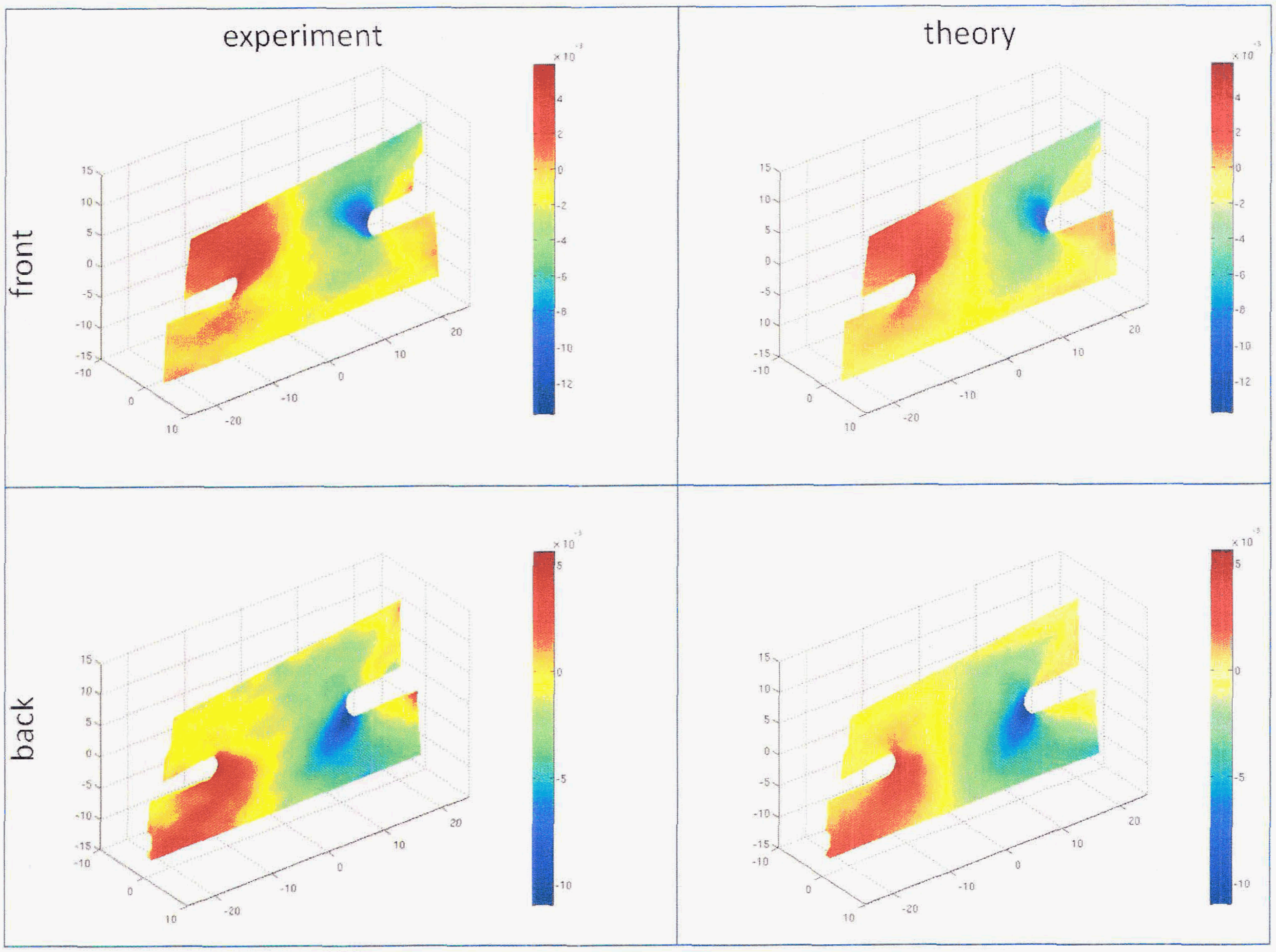

FIGURE 6: COMPARISON OF (ε_{yy}) FIELD BETWEEN MEASURED (LEFT) AND THE IDENTIFIED MODEL BY USING THE FSF FOR THE CASE OF IN-PLANE ROTATION AND TORSION OF A +/- 60 DEGREES LAMINATE

Journal of Computing and Information Science in Engineering, ***11***(2).

[2] Michopoulos, J., Hermanson, J. C., Iliopoulos, A., Lambrakos, S., and Furukawa, T., 2011. "Overview of constitutive response characterization for composite materials via data-driven design optimization". In Proceedings of the ASME 2011 International Design Engineering Technical Conferences & Computers and Information in Engineering Conference IDETC/CIE, August 29-31, 2011, Washington, DC, USA.

[3] Daniel, I. M., and Ishai, O., 2005. *Engineering Mechanics of Composite Materials*, 2nd ed. Oxford University Press, USA, July.

[4] Carlsson, L., Adams, D. F., and Pipes, R. B., 1986. *Experimental Characterization of Advanced Composite Materials, Third Edition*, 3 ed. CRC Press, Dec.

[5] Mast, P., Beaubien, L., Clifford, M., Mulville, D., Sutton, S., Thomas, R., Tirosh, J., and Wolock, I., 1983. "A semi-automated in-plane loader for materials testing". *Experimental Mechanics*, ***23***, pp. 236–241. 10.1007/BF02320415.

[6] Mast, P. W., Nash, G. E., Michopoulos, J. G., Thomas, R. W., Badaliance, R., and Wolock, I., 1992. Experimental determination of dissipated energy density as a measure of strain-induced damage in composites. Tech. Rep. Tec. Rpt. NRL/FR/6383–92-9369, Naval Research Laboratory, Washington, DC, USA.

[7] Mast, P., Nash, G., Michopoulos, J., Thomas, R., Wolock, I., and Badaliance, R., 1995. "Characterization of strain-induced damage in composites based on the dissipated energy density Part I. Basic scheme and formulation". *Theoretical and Applied Fracture Mechanics*, ***22***(2), pp. 71–96.

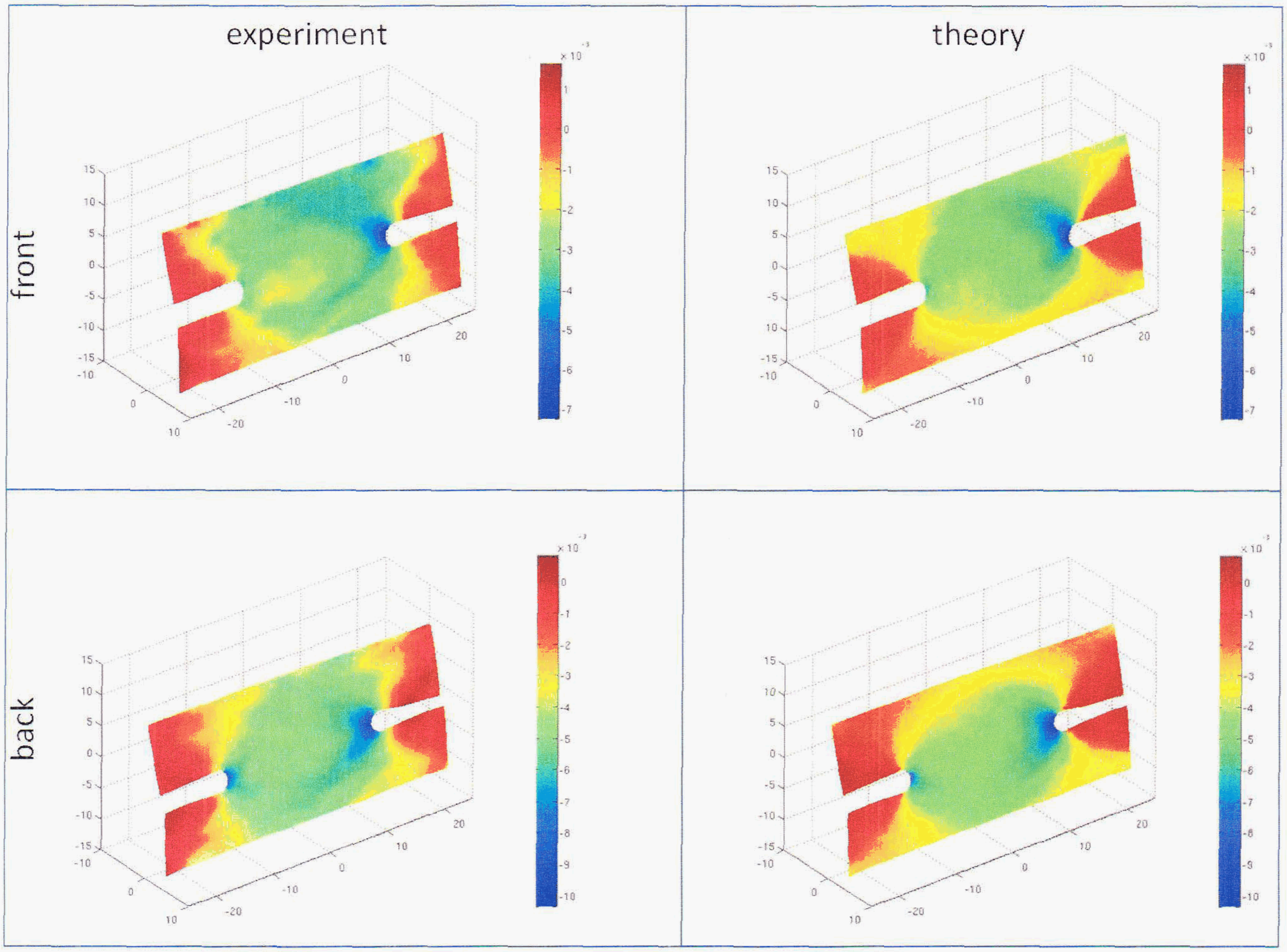

FIGURE 7: COMPARISON OF (ε_{yy}) FIELD BETWEEN MEASURED (LEFT) AND THE IDENTIFIED MODEL BY USING THE FSF FOR THE CASE OF COMPRESSION, BENDING AND NEGATIVE IN-PLANE ROTATION OF A +/- 60 DEGREES LAMINATE

[8] Michopoulos, J., 2003. *Recent advances in Composite Materials: In Honor Of S.A. Paipetis*. Kluwer Academic Press, ch. Computational and Mechatronic Automation of Multiphysics Research for Structural and Material Systems, pp. 9–21.

[9] Michopoulos, J., 2004. "Mechatronically automated characterization of material constitutive respone". In Proceedings of the 6th World Congress on Computational Mechanics (WCCM-VI), Tsinghua University Press and Springer, pp. 486–491.

[10] Michopoulos, J., Hermanson, J., and Furukawa, T., 2008. "Towards the robotic characterization of the constitutive response of composite materials". *Composite Structures, 86*(1-3), pp. 154–164.

[11] Pierron, F., Vert, G., Burguete, R., Avril, S., Rotinat, R., and Wisnom, M. R., 2007. "Identification of the orthotropic elastic stiffnesses of composites with the virtual fields method: Sensitivity study and experimental validation". *Strain, 43*(3), pp. 250–259.

[12] Cooreman, S., Lecompte, D., Sol, H., Vantomme, J., and Debruyne, D., 2007. "Elasto-plastic material parameter identification by inverse methods: Calculation of the sensitivity matrix". *International Journal of Solids and Structures, 44*(13), pp. 4329 – 4341.

[13] Furukawa, T., and Michopoulos, J., 2008. "Computational design of multiaxial tests for anisotropic material characterization". *International Journal for Numerical Methods in Engineering, 74*(12), pp. 1872–1895.

[14] Michopoulos, J. G., Iliopoulos, A. P., and Furukawa, T., 2009. "Accuracy of inverse composite laminate characteri-

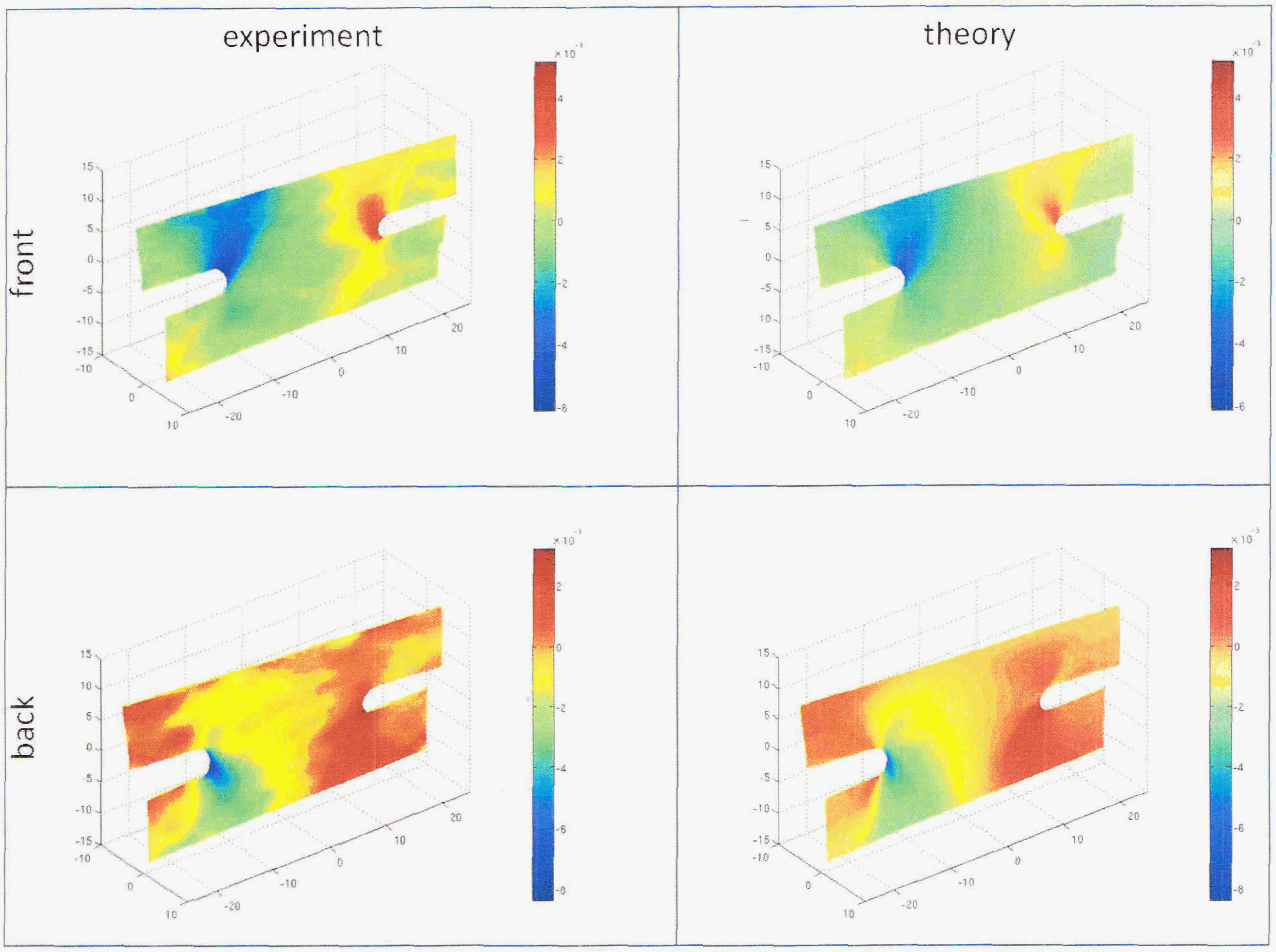

FIGURE 8: COMPARISON OF (ε_{yy}) FIELD BETWEEN MEASURED (LEFT) AND THE IDENTIFIED MODEL BY USING THE FSF FOR THE CASE OF C BENDING, IN-PLANE ROTATION AND TORSION OF A +/- 30 DEGREES LAMINATE WITH 4-PLIES PER LAYER

zation via the mesh free random grid method". *ASME Conference Proceedings*, ***2009***(48999), pp. 367–374.

[15] Bruno, L., Furgiuele, F. M., Pagnotta, L., and Poggialini, A., 2002. "A full-field approach for the elastic characterization of anisotropic materials". *Optics and Lasers in Engineering*, ***37***(4), pp. 417 – 431.

[16] Schmidt, T., Tyson, J., and Galanulis, K., 2003. "Full–field dynamic displacement and strain measurement using advanced 3d image correlation photogrammetry: Part 1". *Experimental Techniques*, ***27***(3), pp. 47–50.

[17] Kajberg, J., and Lindkvist, G., 2004. "Characterisation of materials subjected to large strains by inverse modelling based on in-plane displacement fields". *International Journal of Solids and Structures*, ***41***(13), pp. 3439 – 3459.

[18] Meuwissen, M. H. H., Oomens, C. W. J., Baaijens, F. P. T., Petterson, R., and Janssen, J. D., 1998. "Determination of the elasto-plastic properties of aluminium using a mixed numerical-experimental method". *Journal of Materials Processing Technology*, ***75***(1-3), pp. 204 – 211.

[19] Molimard, J., Le Riche, R., Vautrin, A., and Lee, J., 2005. "Identification of the four orthotropic plate stiffnesses using a single open-hole tensile test". *Experimental Mechanics*, ***45***, pp. 404–411. 10.1007/BF02427987.

[20] Michopoulos, J. G., and Iliopoulos, A. P., 2009. "A computational workbench for remote full field 2d displacement and strain measurements". *ASME Conference Proceedings*, ***2009***(48999), pp. 55–63.

[21] Andrianopoulos, N. P., and Iliopoulos, A. P., 2006. "Displacements measurement in irregularly bounded plates using mesh free methods". In Proc. 16th European Confer-

ence of Fracture, Alexandroupolis, Greece, July 3–7.

[22] Iliopoulos, A. P., Michopoulos, J. G., and Andrianopoulos, N. P., 2008. "Performance sensitivity analysis of the Mesh-Free Random Grid method for whole field strain measurements". *ASME Conference Proceedings, **2008***(43277), pp. 545–555.

[23] Iliopoulos, A. P., Michopoulos, J. G., and Andrianopoulos, N. P., 2010. "Performance analysis of the Mesh-Free Random Grid Method for full-field synthetic strain measurements". *Strain*, p. In Print.

[24] Iliopoulos, A., and Michopoulos, J., 27–31 Jul 2009. "Sensitivity analysis of the mesh-free random grid method for measuring deformation fields on composites". In Proceedings of the 17th International Conference on Composite Materials, ICCM-17, Edinburgh, The British Composites Society: Edinburgh International Convention Centre (EICC), Edinburgh, UK, 2009.

[25] Iliopoulos, A. P., and Michopoulos, J. G., 2009. "Effects of anisotropy on the performance sensitivity of the Mesh-Free random grid method for whole field strain measurement". *ASME Conference Proceedings, **2009***(48999), Jan., pp. 65–74.

[26] Michopoulos, J. G., Hermanson, J. C., and Iliopoulos, A., 2010. "Towards a recursive hexapod for the multidimensional mechanical testing of composites". In Proceedings of the ASME 2010 International Design Engineering Technical Conferences & Computers and Information in Engineering Conference IDETC/CIE 2010, no. DETC2010/CIE-28699.

[27] Michopoulos, J., and Furukawa, T., 2007. "Multi-level coupling of dynamic data-driven experimentation with material identification". *Lecture Notes in Computer Science (including subseries Lecture Notes in Artificial Intelligence and Lecture Notes in Bioinformatics), **4487 LNCS***, pp. 1180–1188.

[28] Furukawa, T., Michopoulos, J., and Kelly, D., 2008. "Elastic characterization of laminated composites based on multiaxial tests". *Composite Structures, **86***(1-3), pp. 269–278.

[29] Man, H., Furukawa, T., and Kellermann, D., 2008. "Implicit constitutive modeling based on the energy principles". In Proceedings of XXII ICTAM, 25-59 August 2008, Adelaide 2008.

[30] Furukawa, T., and Michopoulos, J., 2008. "Online planning of multiaxial loading paths for elastic material identification". *Computer Methods in Applied Mechanics and Engineering, **197***(9-12), pp. 885–901.

[31] Michopoulos, J., Furukawa, T., and Lambrakos, S., 2009. "Data-driven characterization of composites based on virtual deterministic and noisy multiaxial data". In 2008 ASME International Design Engineering Technical Conferences and Computers and Information in Engineering Conference, DETC 2008, Vol. 3, pp. 1095–1106.

[32] Furukawa, T., and Pan, J. W., 2010. "Stochastic identification of elastic constants for anisotropic materials". *International Journal for Numerical Methods in Engineering, **81***(4), pp. 429–452.

[33] Haj-Ali, R., and Kim, H.-K., 2007. "Nonlinear constitutive models for FRP composites using artificial neural networks". *Mechanics of Materials, **39***(12), pp. 1035 – 1042.

[34] Haupt, P., 2002. *Continuum Mechanics and Theory of Materials*, 2nd ed. Springer, Apr.

[35] Van Der Meer, F., and Sluys, L., 2009. "Continuum models for the analysis of progressive failure in composite laminates". *Journal of Composite Materials, **43***(20), pp. 2131–2156.

[36] Ju, J. W., Chaboche, J., and Voyiadjis, G. Z., 1998. *Damage Mechanics in Engineering Materials*, 1st ed. Elsevier Science, Jan.

[37] Kaliske, M., 2000. "A formulation of elasticity and viscoelasticiy for fibre reinforced material at small and finite strains". *Comput. Meth. Appl. Mech. Eng., **185***, pp. 225–243.

[38] Michopoulos, J., and Iliopoulos, A., 2011. "A computational workbench for remote full field 3d displacement and strain measurements". In Proceedings of the ASME 2011 International Design Engineering Technical Conferences & Computers and Information in Engineering Conference IDETC/CIE, August 29-31, 2011, Washington, DC, USA.

[39] Jones, D. R., Perttunen, C. D., and Stuckman, B. E., 1993. "Lipschitzian optimization without the Lipschitz constant". *J. Optim. Theory Appl., **79***(1), pp. 157–181.

[40] The Mathworks. Matlab. http://www.mathworks.com.

[41] Iliopoulos, A. P., and Michopoulos, J. G., 2010. "Loading subspace selection for multidimensional characterization tests via computational experiments". *ASME Conference Proceedings, **2010***(44113), pp. 101–110.

[42] Michopoulos, J., C., H. J., and Iliopoulos, A., 2012. "Robotic and multiaxial testing for the constitutive characterization of composites". In Materials Challenges in Alternative & Renewable Energy, February 26-March 1, 2012, Clearwater, FL, USA.